Hindawi
Scientific Programming
Volume 2021, Article ID 4016914, 8 pages
https://doi.org/10.1155/2021/4016914

Research Article

Analysis of Image Features and TCM Syndrome Types of Lobar Pneumonia in Children Based on Mean Square Deviation Lung CT Image Registration Algorithm

Shuang Wang, Yi Zhang, and Yongkun Liu

Department of Pediatrics, Huangdao District Hospital of Traditional Chinese Medicine, Qingdao 266500, Shandong, China

Correspondence should be addressed to Yongkun Liu; 3115706002@m.fafu.edu.cn

Received 7 June 2021; Revised 24 June 2021; Accepted 13 July 2021; Published 23 July 2021

Academic Editor: Gustavo Ramirez

The aim was to analyze the application of computed tomography (CT) images in the diagnosis of lesions, and the composition of traditional Chinese medicine (TCM) syndromes in children with lobar pneumonia. Lung CT image registration algorithm was constructed based on optimized mean square deviation (OMSD) algorithm, which was applied to CT images of 188 children patients with lobar pneumonia before and after treatment. Besides, free-form deformation (FFD) algorithm and mean square deviation (MSD) algorithm were introduced for comparison with OMSD. Results showed that sum of squared differences (SSD) of OMSD was significantly lower than that of MSD and FFD ($P < 0.05$). The mutual information (MI), relative overlap rate (ROR), and r_{cc} of OMSD were markedly higher than those of MSD and FFD ($P < 0.05$). After treatment, the number of pulmonary interstitial thickening, lobular interstitial thickening, ground-glass shadow, patchy shadow, consolidation shadow, pleural thickening, pleural effusion, lymphadenopathy, pneumothorax, and mediastinal emphysema decreased sharply in contrast to before treatment ($P < 0.05$). Among the selected children, there were 184 children patients with empirical TCM syndrome, accounting for 97.85%, and its dominant syndrome was wind-heat closed lung syndrome (52.75%) and phlegm-heat closed lung syndrome (46.11%). The main symptoms of wind-heat closed and phlegm-heat closed lung syndrome were fever, cough, and pulmonary rales. In conclusion, OMSD was superior to MSD and FFD in lung CT image registration. CT registration image based on OMSD could clearly display the intrapulmonary and extrapulmonary manifestations of children patients, so as to enhance the clinical diagnosis effect. Besides, wind-heat closed lung syndrome and phlegm-heat closed lung syndrome were the common types of TCM syndrome of children pneumonia with the common symptoms of fever and cough.

1. Introduction

Pneumonia is one of the most common infectious diseases among children around the world. Bacteria can directly enter the lungs to change the inflammation in lungs, because children are underdeveloped and had relatively short tracheas [1]. Statistical data from the World Health Organization (WHO) show that about 3 million children die from pneumonia each year. Therefore, pneumonia is a serious threat to children's physical and mental health. Besides, pneumonia can be divided into lobar pneumonia, lobular pneumonia, and interstitial pneumonia based on the anatomical sites. Lobar pneumonia, also known as alveolar pneumonia or pneumococcus pneumonia, is an inflammation mainly caused by the pneumococcus with diffuse cellulose exudation among alveoli [2, 3]. Clinically, its onset is rapid, and typical manifestations are high fever, chills, chest pain, cough, cough of rusty sputum, difficult breathing, etc. Lobular pneumonia may also cause pulmonary fleshiness, pleural hypertrophy and adhesion, pulmonary abscess and empyema, sepsis, septic shock, and other complications during the pathogenesis [4, 5].

With the development of medical imaging, X-ray plain film, CT, and other imaging techniques have been gradually applied in the diagnosis of lobar pneumonia in children by chest routine scan [6]. Besides, the increased lung markings or involved pulmonary segment and slightly blurred lung lobe are only observed at the early X-ray plain film. As the lesions progressed, the alveoli were filled with inflammatory

exudates, and X-ray plain film presents as large areas of inflammatory infiltration shadows or consolidation. Unfortunately, there are high misdiagnosis and missed diagnosis by using X-ray plain film. Compared with X-ray plain film, CT image has a higher density resolution, can detect lesions earlier, and has the advantages of simple operation, no traumatic, and low price [7]. In the actual scanning, organs will become unconsciously deformed due to inevitable breathing movement, resulting in the difference in image quality, which involves the image registration technology. Medical image registration is a basic subject of medical image analysis, which plays a very vital role in diagnosing diseases and making treatment plans for diseases. The MSD measurement is mainly applied in single-mode image registration, which has a low computational complexity to greatly reduce the image registration time. However, it is easy to fall into the dilemma of local extremum, which affects the registration accuracy [8]. Burgmans et al. [9] had a fusion registration automatically and manually for CT and ultrasound images of liver interventional therapy and found that the average displacement of superficial and deep liver lesions in images after manual registration was better greatly than that after automatic registration. Wang et al. [10] proposed a homomodal nonrigid medical image registration algorithm based on adaptive difference that was applied in the lung CT images. They found that this method could deal with the nonrigid registration of the same morphological medical image, which had the application prospect of diagnostic imaging. Therefore, the CT image registration algorithm was established in this study through improving MSD measurement.

To sum up, lung CT image registration algorithm was constructed based on OMSD and compared with FFD and MSD. Lung CT image registration algorithm was applied to CT images of 188 children patients with lobar pneumonia before and after treatment, so as to comprehensively explore the CT image characteristics and TCM syndrome of children patients with lobar pneumonia.

2. Materials and Methods

2.1. Sample Selection. 188 children patients with 3–12 years of age were selected as the subjects to be investigated, who were admitted to hospital from January 5, 2018, to January 30, 2020, and diagnosed with lobar pneumonia. The experiment had been approved by the Medical Ethics Committee of hospital, and the family members of children patients had been informed of this experiment and signed the informed consents.

The criteria for inclusion were defined to include children patients who had complete clinical medical records and basic data, had no contraindication of CT scan, have not received relevant treatment before examination, and informed their family members to agree to experiment.

The criteria for exclusion were defined to include children patients who suffered from coagulation dysfunction, malignant tumors, and other respiratory infectious diseases.

2.2. Computed Tomography Scanning. A 64-slice spiral CT machine (produced by Toshiba, Japan) was employed to examine the children patients. They were in the supine position with arms raised above the head and scanned from the lung tip to the diaphragm. If one child was in a bad mood, the child's family members could accompany him or her throughout the whole examination. The scan parameters were as follows. The tube voltage was 120 kV, tube current is 80–120 mAs, pitch was 0.957 : 1, interval was 0.615 mm, thickness of slice was 5 mm, slice gap was 5 mm, and matrix was 521×521. After scan was completed, the obtained image was sent to the workstation.

2.3. Lung CT Image Registration Algorithm Based on Optimized Mean Square Deviation. Registration technique was an important part of medical image processing. First, a floating image was for feature extraction, spatial transformation, and interpolation; and then, the similarity was tested with a reference image to judge whether the test result was optimal strategy. If the result was optimal strategy, image registration could be output; if not, the image should be optimized by the best strategy, and it would be operated by registration again until it could be output, as shown in Figure 1.

The image registration process was actually to find the optimal transformation parameters, and a moving image was mapped to the corresponding position of the fixed image through the spatial transformation parameters. It was assumed that a voxel coordinate in the image domain was $X = [X_1, X_2, X_3]^T$, conversion parameter is f, and then, the registration problem was converted to the minimum value solution problem, as shown in the following equation.

$$\overline{\overline{\vartheta}} = \arg\min D\left(\vartheta\colon H_G, H_J\right). \tag{1}$$

In equation (1), I_G expressed a point of a fixed image, I_J represented a point of a moving image, D expressed the cost function, and ϑ stood for deformation vector parameter. The ultimate goal of image registration was to ensure image similarity, so the selection of measurement was extremely important in the process. Therefore, MSD measurement was adopted for a wide range of dynamic search and matching. Then, the calculation equation could be as follows.

$$\mathrm{MSD} = \frac{\sum_{(x,y)\in\Psi} (G(x,y) - J(x,y))^2}{\Psi}. \tag{2}$$

In equation (2), G and J expressed a fixed image and a floating image, respectively; Ψ represented an area to be registered, $G(x, y)$ stood for a grey level of pixel corresponding to the fixed image in (x, y), and $J(x, y)$ expressed a grey level of pixel corresponding to the floating image in (x, y). Besides, MSD meant the alignment standard between two images; the higher the value of MSD, the lower the image similarity. However, MSD lacked matching accuracy, so that the processing of image edge was not smooth enough. Thus, several measurements were combined in the study, and their configuration cost function was shown as follows:

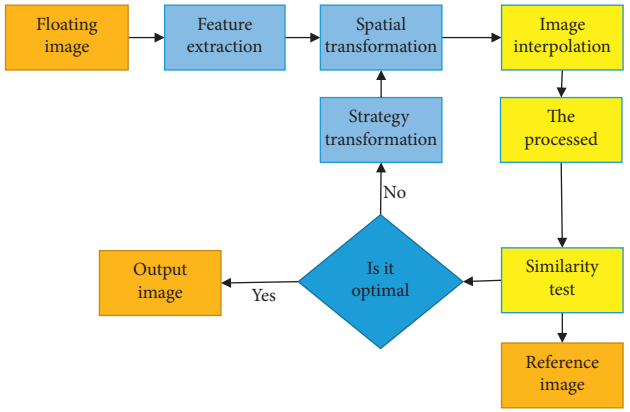

Figure 1: Flow chart of image registration.

$$C\left(T_\vartheta: H_G, H_J\right) = \frac{1}{\sum_{i=1}^{N} w_i} \sum_{i=1}^{N} w_i C_i\left(T_\vartheta: H_G, H_J\right). \quad (3)$$

In equation (3), w_i, C_i, and T_ϑ represented the weight value of image algorithm, cost function, and spatial transformation parameter, respectively. In order to further limit the size of spatial transformation, penalty term was introduced into the cost function, as shown in the following equation:

$$C = \lambda_1 S + \lambda_2 P(\vartheta). \quad (4)$$

In equation (4), $P(\vartheta)$ stood for penalty factor, λ_1 and λ_2 were both custom constants, and S expressed MSD registration algorithm. Therefore, the above was OMSD image registration algorithm. The whole flow is shown in Figure 2.

2.4. Evaluation Indexes of Lung Image Registration Algorithm. The nonrigid registration algorithm under FFD [11] and the traditional nonrigid registration algorithm under MSD [12] were introduced for comparison with OMSD image registration algorithm. Therefore, the above comparison should be evaluated by SSD, MI, ROI, and r_{cc}.

SSD expressed a grey value of one point in fixed and floating images, and the less the value of SSD, the better the image registration effect. It could be calculated as follows:

$$\mathrm{SSD} = \frac{1}{\|\psi\|} \sum_{x \in \psi} \left(f_t(\varphi(X)) - f_s(X)\right)^2. \quad (5)$$

In equation (5), f_t represented a grey value of a fixed image, f_s expressed a grey value of a floating image, $\varphi(X)$ stood for a coordinate after an image was deformed, and ψ meant an area to be registered.

MI expressed the similarity of registration domain, and the bigger the value of MI, the higher the similarity of image. It could be expressed as the following equation:

$$\mathrm{MI} = H(G) + H(J) - H(G, J). \quad (6)$$

In equation (6), $H(G)$ and $H(J)$ stood for information entropy of a fixed image and a floating image, respectively; and $H(G, J)$ represented a combined information entropy of fixed and floating images.

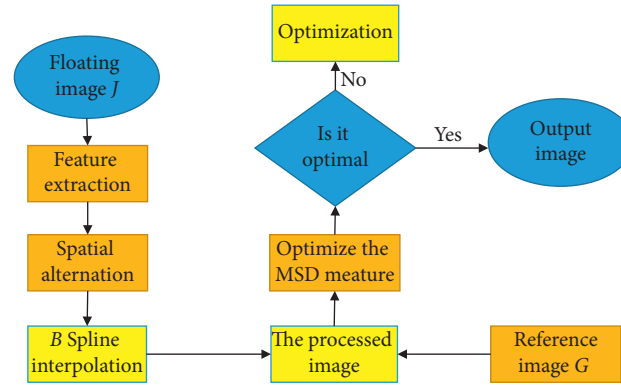

Figure 2: Flow chart of OMSD image registration algorithm.

ROI expressed the degree of alignment in registration domain, and the higher the value of ROI, the better the registration effect. It could be calculated as follows:

$$\mathrm{ROI}(P, S) = \frac{V(P, S)}{V(P, S)}. \quad (7)$$

In equation (7), P and S stood for the corresponding pulmonary segmented regions.

r_{cc} represented the correlation of images, and the bigger the value of r_{cc}, the higher the correlation of images.

$$r_{cc} = \frac{\sum_{i=0}^{M-1} (r_i - \overline{r})(c_i - \overline{c})}{\left[\sqrt{\sum_{i=0}^{M-1} (r_i - \overline{r})} \sqrt{\sum_{i=0}^{M-1} (c_i - \overline{c})^2}\right]}. \quad (8)$$

In equation (8), M expressed the number of pixels in an image. In addition, $\overline{r}$ and $\overline{c}$ stood for average grey value of images.

2.5. Observation Indexes. Basic data of patients (age ratio and gender ratio) were recorded. What is more, CT image characteristics of the lungs before and after treatment were recorded, including intrapulmonary characteristics (pulmonary interstitial thickening, lobular interstitial thickening, ground-glass shadow, patchy shadow, and consolidation shadow) and extrapulmonary characteristics (pulmonary interstitial thickening, lobular interstitial thickening, ground-glass shadow, patchy shadow, and consolidation shadow).

2.6. Statistical Methods. SPSS19.0 version statistical software was adopted to analyze and process the experimental data, measurement data was expressed as the mean ± standard deviation ($\overline{x} \pm s$), and enumeration data was represented as percentage (%). The paired t-test was applied to compare SSD, MI, ROI, and r_{cc} of OMSD, MSD, and FFD. The variance was for analysis of comparison on the number of intrapulmonary and intrapulmonary CT images of children patients before and after treatment. $P < 0.05$ meant that the difference was statistically significant.

3. Results

3.1. Basic Information of the Selected Children Patients. Figure 3 shows the basic information of selected children patients. As for gender, the proportion of male children patients (58.81%) was greatly higher than that of female children patients (41.19%). In addition, the proportion of children patients with the age of 3–6 years old was highest (47.82%), followed by children patients aged 6–9 years (33.05%) and aged 9–12 years (19.13%).

Figures 4(a) and 4(b) are CT images of the pulmonary window and mediastinal window of a male child patient, respectively, showing a large patchy high-density shadow in the middle lobe of right lung, and there was aerated bronchus syndrome in it. Lung consolidation was big lobular or occupied the shadow that was consistent with increasing density in most of the lobes, which could be regarded as the consolidation stage of lobar pneumonia. Figures 4(c) and 4(d) are CT images of the pulmonary window and mediastinal window of a female child patient, respectively. It revealed that right lung volume shrunk; hilum of right lung displayed patchy shadow; lobar bronchus was congested with low density, and no enhancement, which displayed dotted high-density calcification, and its peripheral of lesion extended; the inferior lobe of right lung had a large patch of dense shadows, blood vessels in it were deformed naturally, and it expressed atelectasis change. In addition, Figures 4(e) and 4(f) are CT images of the pulmonary window and mediastinal window of a male child patient, respectively. It showed that nodules were observed in the right lower lung with uneven density and coarse contour; and there were lobules and pleural indentation gathered with large amounts of blood vessels. The lesions were big lobular or distributed in lung segments. There were clear bronchogenic shadows within the lesions with the edges restricted and straight by the pleura.

3.2. Traditional Chinese Medicine Syndrome and Main Symptom Distribution in Children Patients. As shown in Figure 5, there were 184 children patients with excessive syndrome of TCM (97.85%) and 4 children patients with deficient syndrome (2.15%). Among the children patients with excessive syndrome of TCM, the proportion of children patients with wind-heat closed lung syndrome was the highest (52.75%) followed by the proportion of children patients with phlegm-heat closed lung syndrome (46.11%), and the proportion of other syndromes (wind-cold closed lung syndrome, cold-heat complicated syndrome, and phlegm-damp closed lung syndrome) was very low (1.14%). In addition, the proportion of children patients with spleen deficiency syndrome with phlegm accumulation was the highest (63.16%), followed by lung-spleen qi deficiency syndrome (36.84%).

Figure 5 indicates that the wind-heat closed lung syndrome and phlegm-heat closed lung syndrome were dominant in children patients with excessive syndrome, while the other syndromes were all low-probability, so only the number of children patients with wind-heat closed lung syndrome and phlegm-heat closed lung syndrome was used for statistics. As shown in Figure 6, the main symptoms of children patients with wind-heat closed lung syndrome and phlegm-heat closed lung syndrome were fever, cough, and pulmonary rales, with less phlegm and asthma.

3.3. Comparison on Image Registration Effects of the Three Algorithms. As shown in Figures 7 and 8, the SSD of OMSD was 0.078, MI was 0.957, ROI was 0.804, and r_{cc} was 0.921; the SSD, MI, ROI, and r_{cc} of FFD were 0.126, 0.861, 0.655, and 0.836, respectively; and the SSD of MSD was 0.118, MI was 0.849, ROI was 0.681, and r_{cc} was 0.817. In addition, the SSD of OMSD was sharply lower than that of MSD and FFD, and the difference was statistically substantial ($P < 0.05$). The MI, ROI, and r_{cc} of OMSD were markedly higher than those of MSD and FFD, and there were statistically great differences ($P < 0.05$).

3.4. Computed Tomography Findings of Children Patients before and after Treatment. Figure 9 demonstrates that H1, H2, H3, H4, H5, H6, H7, H8, H9, and H10 expressed interstitial lung thickening, pulmonary interstitial thickening, lobular interstitial thickening, ground-glass shadow, patchy shadow, consolidation shadow, pleural thickening, pleural effusion, lymphadenopathy, pneumothorax, and mediastinal emphysema, respectively. After treatment, the number of H1, H2, H3, H4, H5, H6, H7, H8, H9, and H10 in children patients was dramatically lower than that before treatment, showing a statistically marked difference ($P < 0.05$).

4. Discussion

Lobar pneumonia is one of the pathologic categories of pneumonia in children and is also a very common respiratory disease. In clinical practice, CT images are usually applied to diagnose lobular pneumonia in children. However, the medical images may cause problems in the quality due to the influence of various objective factors [13]. Therefore, lung CT image registration algorithm was established based on OMSD, and FFD and MSD were introduced for comparison with OMSD. The results showed that the SSD of OMSD was steeply lower than that of MSD and FFD ($P < 0.05$), which was different with the research results of Yang et al. [14] due to the different performances of registration algorithms. The quality of CT image registered by OMSD was obviously better than that of MSD and FFD. The MI, ROI, and r_{cc} of OMSD were remarkably higher than those of MSD and FFD, and the differences were statistically great ($P < 0.05$), which also indicated that OMSD was superior to MSD and FFD in lung CT image registration [15]. OMSD was applied to CT images of 188 children patients with lobar pneumonia before and after treatment. It was found that the number of pulmonary interstitial thickening, lobular interstitial thickening, ground-glass shadow, patchy shadow, consolidation shadow, pleural thickening, pleural effusion, lymphadenopathy, pneumothorax, and mediastinal emphysema in children patients after treatment decreased dramatically in contrast to that before treatment ($P < 0.05$).

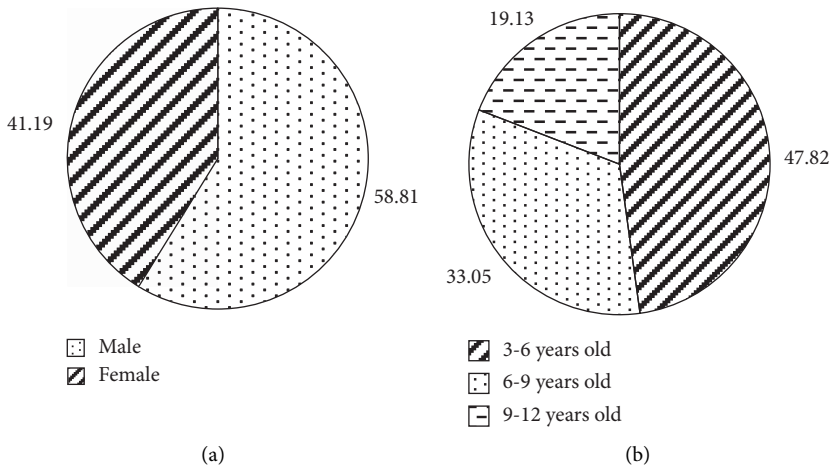

Figure 3: Basic information of the selected children patients: (a) The gender ratio of children patients; (b) The age ratio of children patients.

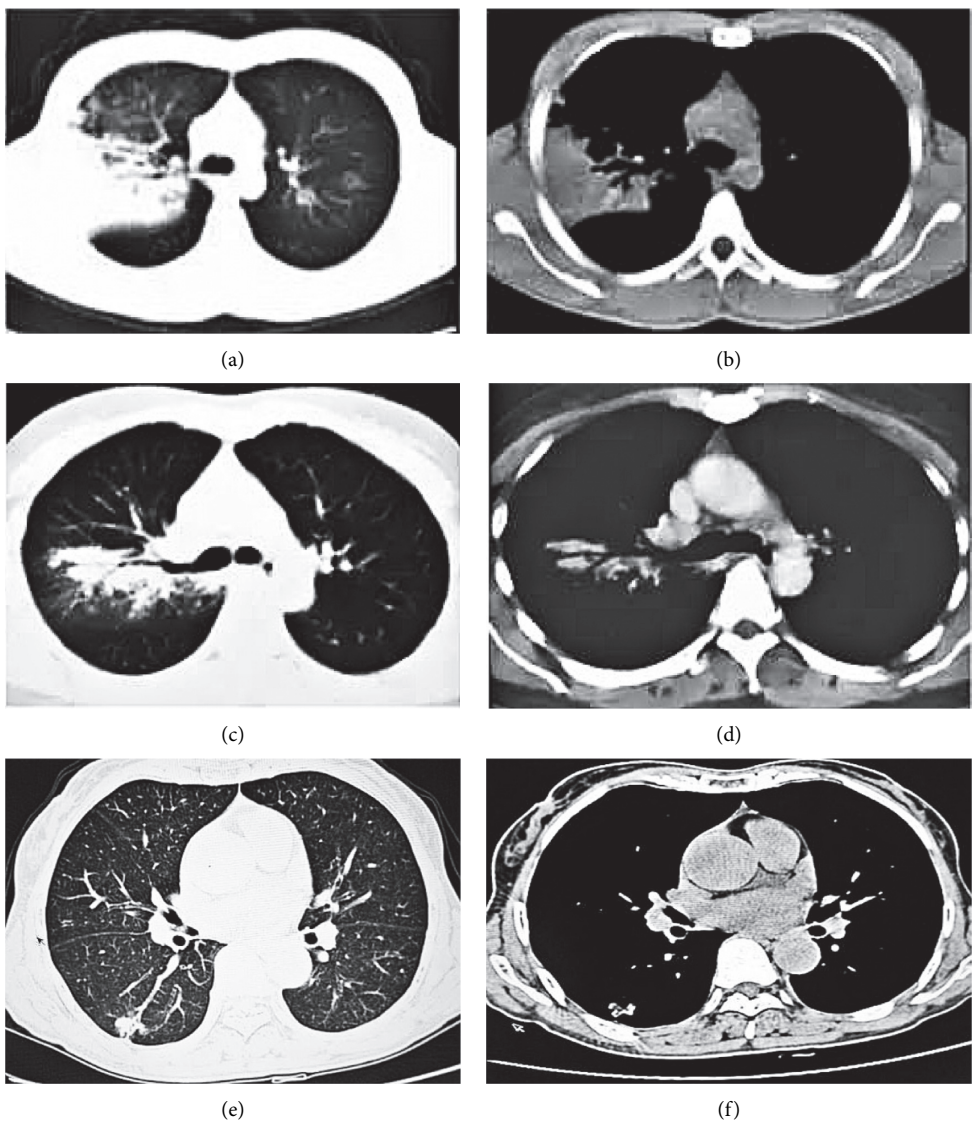

Figure 4: MRI images of children patients with lobar pneumonia: (a, b) CT images of the pulmonary window and mediastinal window of a male child patient (aged 5 years), respectively; (c, d) CT images of the pulmonary window and mediastinal window of a female child patient (aged 11 years), respectively; (e, f) CT images of the pulmonary window and mediastinal window of a male child patient (aged 12 years).

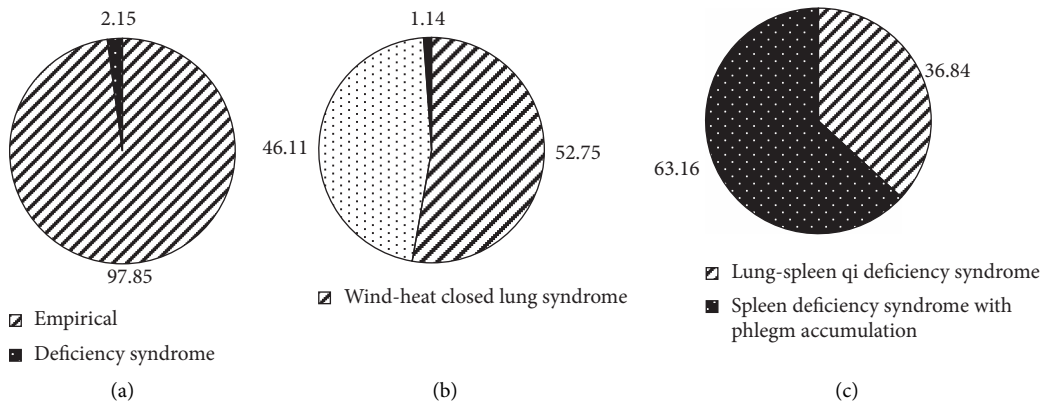

Figure 5: Composition of TCM syndromes in children patients: (a) The ratio of the number of excessive syndrome and deficient syndrome in children patients; (b) The composition of excessive syndrome in children patients; (c) The constitution of deficient syndrome in children patients.

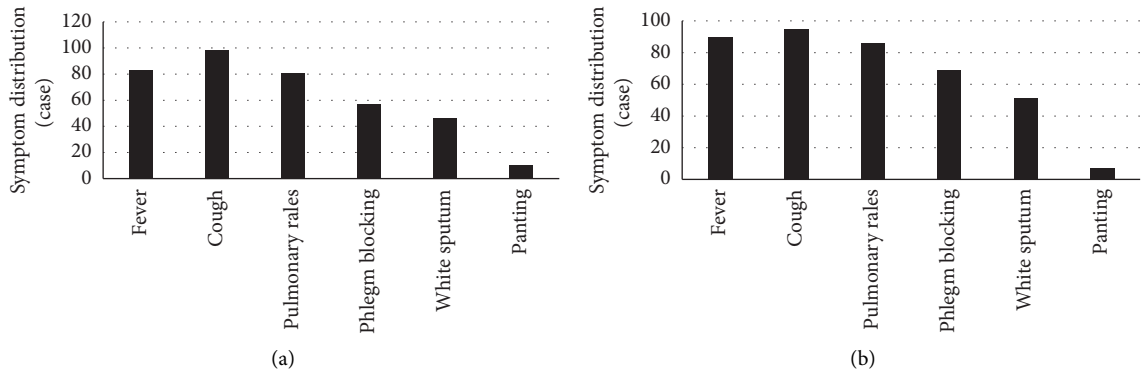

Figure 6: The symptom distribution of children patients with wind-heat closed lung syndrome and phlegm-heat closed lung syndrome: (a) The symptom distribution of children patients with wind-heat closed lung syndrome; (b) The symptom distribution of children patients with phlegm-heat closed lung syndrome.

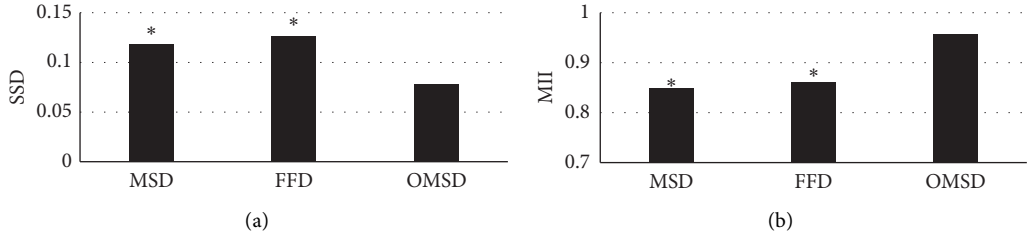

Figure 7: Comparison on the SSD and MI of the three algorithms: * denotes that there was statistical meaning ($P < 0.05$) in contrast to OMSD).

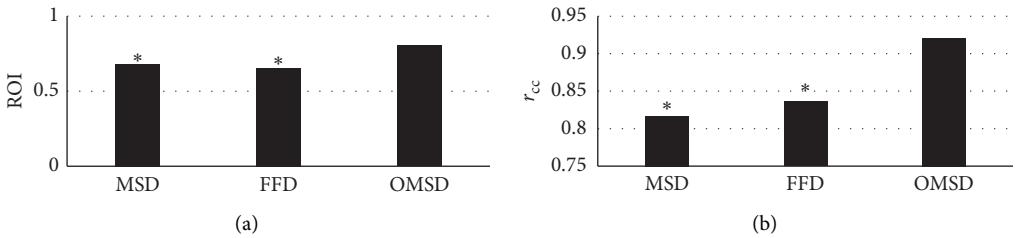

Figure 8: Comparison on the ROI and r_{cc} of the three algorithms: * denotes that there was statistical meaning ($P < 0.05$) in contrast to OMSD.

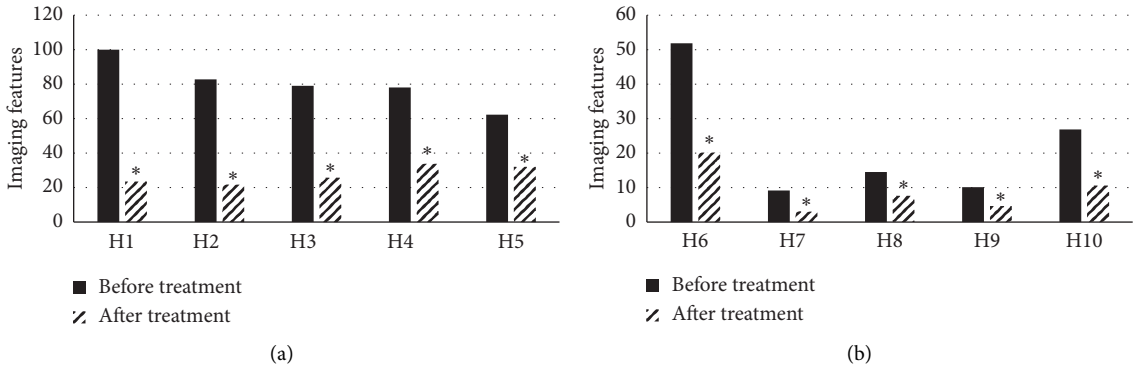

Figure 9: Intrapulmonary and extrapulmonary CT findings of children patients before and after treatment: (a) expressed the intrapulmonary manifestations of children patients before and after treatment; and (b) stood for the extrapulmonary manifestations of children patients before and after treatment. * denotes that the meaning was statistical ($P < 0.05$) in contrast to before treatment.

Therefore, it indicated that CT image registration based on OMSD could clearly display the intrapulmonary and extrapulmonary manifestations of children patients to improve the effect of clinical diagnosis.

The study on TCM syndrome of lobar pneumonia can not only clarify its pathogenic cause and position, but also provide reference for clinical identification. There were 184 cases with TCM excessive syndrome among the selected children accounting for 97.85%, and 4 cases with deficient syndrome accounting for 2.15%. In addition, wind-heat closed lung syndrome (52.75%) and phlegm-heat closed lung syndrome (46.11%) were dominant in the excessive syndrome, which was not consistent with the research results of Upchurch et al. [16] in the adult patients with pneumonia. This was because of the different types of pneumonia and medical syndrome. Therefore, the results showed that the remaining syndrome was small probability events. Thus, it illustrated that wind-heat closed lung syndrome and phlegm-heat closed lung syndrome were the most common TCM syndromes of children's pneumonia. The main symptoms of wind-heat closed lung syndrome and phlegm-heat closed lung syndrome were fever, cough, and pulmonary rales, and the proportion of phlegm and asthma symptoms was relatively small, which was consistent with the research results of Liszewski et al. [17], suggesting that fever and cough were common in the two syndromes.

5. Conclusion

Lung CT image registration algorithm was constructed based on OMSD, and FFD and MSD were introduced for comparison with OMSD, so as to apply to CT images of 188 children patients with lobar pneumonia before and after treatment. The results showed that OMSD was better than MSD and FFD in lung CT image registration. CT registration image based on OMSD could clearly display the intrapulmonary and extrapulmonary manifestations of children patients, so as to improve the clinical diagnosis effect. Wind-heat closed lung syndrome and phlegm-heat closed lung syndrome were the common TCM syndromes of children pneumonia with fever and cough as their common symptoms. However, the optimization of registration algorithm in this study was mainly in MSD measurement, and the rest of the process was not discussed. The interpolation algorithm of registration process would be discussed in the future. In short, the mean square error was innovatively optimized in this study, so as to provide a theoretical basis for the clinical diagnosis and treatment of children patients with lobar pneumonia.

Data Availability

No data were used to support this study.

Conflicts of Interest

The authors declare that there are no conflicts of interest regarding the publication of this paper.

References

[1] J. Le Bel, T. Pelaccia, P. Ray et al., "Impact of emergency physician experience on decision-making in patients with suspected community-acquired pneumonia and undergoing systematic thoracic CT scan," *Emergency Medicine Journal*, vol. 36, no. 8, pp. 485–492, 2019.

[2] T. Yamamoto, M. S. Kent, E. R. Wisner et al., "Single-energy computed tomography-based pulmonary perfusion imaging: proof-of-principle in a canine model," *Medical Physics*, vol. 43, no. 7, pp. 3998–4007, 2016.

[3] D. Pannu, D. Yang, P. L. Abbitt, and P. V. Draganov, "Prospective evaluation of CT esophagram findings after peroral endoscopic myotomy," *Gastrointestinal Endoscopy*, vol. 84, no. 3, pp. 408–415, 2016.

[4] R. Khatib, Y. A. Arevalo, M. A. Berendsen, S Prabhakaran, and M. D Huffman, "Presentation, evaluation, management, and outcomes of acute stroke in low- and middle-income countries: a systematic review and meta-analysis," *Neuroepidemiology*, vol. 51, no. 1-2, pp. 104–112, 2018.

[5] T. Egan, J. Blackwell, and K Birchard, "Assessment of lungs for transplant recovered from uncontrolled donation after circulatory determination of death donors," *Annals of the American Thoracic Society*, vol. 14, no. 3, p. S251, 2017.

[6] D. Wen, L. Wu, and Y Dong, "The effect of acupuncture on the quality of life of patients recovering from COVID-19: a

systematic review protocol," *Medicine*, vol. 99, no. 30, Article ID e20780, 2020.

[7] C. Zhang, J. Li, Z. Wu et al., "Efficacy and safety of Anluohuaxian in the treatment of patients with severe Coronavirus disease 2019- a multicenter, open label, randomized controlled study: a structured summary of a study protocol for a randomised controlled trial," *Trials*, vol. 21, no. 1, p. 495, 2020.

[8] H. X. Bai, B. Hsieh, Z. Xiong et al., "Performance of radiologists in differentiating COVID-19 from non-COVID-19 viral pneumonia at chest CT," *Radiology*, vol. 296, no. 2, pp. E46–E54, 2020.

[9] M. C. Burgmans, J. M. den Harder, P. Meershoek et al., "Phantom study investigating the accuracy of manual and automatic image fusion with the GE logiq E9: implications for use in percutaneous liver interventions," *CardioVascular and Interventional Radiology*, vol. 40, no. 6, pp. 914–923, 2017.

[10] C. Wang, Q. Ren, X. Qin, and Y. Yu, "The same modality medical image registration with large deformation and clinical application based on adaptive diffeomorphic multi-resolution demons," *BMC Medical Imaging*, vol. 18, no. 1, p. 21, 2018.

[11] N. Tanaka, Y. Kunihiro, T. Kobayashi et al., "High-resolution CT findings of idiopathic pneumonia syndrome after haematopoietic stem cell transplantation: based on the updated concept of idiopathic pneumonia syndrome by the American Thoracic Society in 2011," *Clinical Radiology*, vol. 71, no. 10, pp. 953–959, 2016.

[12] M. Carotti, F. Salaffi, P. Sarzi-Puttini et al., "Chest CT features of coronavirus disease 2019 (COVID-19) pneumonia: key points for radiologists," *La radiologia medica*, vol. 125, no. 7, pp. 636–646, 2020.

[13] C. Kloth, W. M. Thaiss, R. Beck et al., "Potential role of CT-textural features for differentiation between viral interstitial pneumonias, pneumocystis jirovecii pneumonia and diffuse alveolar hemorrhage in early stages of disease: a proof of principle," *BMC Medical Imaging*, vol. 19, no. 1, p. 39, 2019.

[14] F. Yang, M. Ding, and X. Zhang, "Non-rigid multi-modal 3D medical image registration based on foveated modality independent neighborhood descriptor," *Sensors*, vol. 19, no. 21, p. 4675, 2019.

[15] H. X. Bai, R. Wang, Z. Xiong et al., "Artificial intelligence augmentation of radiologist performance in distinguishing COVID-19 from pneumonia of other origin at chest CT," *Radiology*, vol. 296, no. 3, pp. E156–E165, 2020.

[16] C. P. Upchurch, C. G. Grijalva, R. G. Wunderink et al., "Community-acquired pneumonia visualized on CT scans but not chest radiographs," *Chest*, vol. 153, no. 3, pp. 601–610, 2018.

[17] M. C. Liszewski, S. Görkem, K. S. Sodhi, and E. Y. Lee, "Lung magnetic resonance imaging for pneumonia in children," *Pediatric Radiology*, vol. 47, no. 11, pp. 1420–1430, 2017.